Theor Chem Acc (1997) 96:141–145

Theoretical
Chemistry Accounts

Letter

On the reduced and oxidized forms of the FeMo- cofactor of *Azotobacter vinelandii* nitrogenase

Krassimir K. Stavrev, Michael C. Zerner

Quantum Theory Project, University of Florida, Gainesville, FL 32611-8435, USA

Received: 19 March 1997 / Accepted: 8 May 1997

Abstract. Reduced and oxidized forms of the FeMo-cofactor of *Azotobacter vinelandii* nitrogenase are examined theoretically within the intermediate neglect of differential overlap model. The results obtained favor one of the experimentally suggested modes of contraction of the metal system which results in an expansion of the central cavity of the cofactor. The bond index analysis indicates marked changes in the Mo coordination upon electron addition which may contribute to an opening of the Mo atom as a possible binding site at the advanced stages of the reduction process. In this work we also compare the 39- and 41-electron [$MoFe_7$] core as possible native resting states, both compatible with known spin and Mössbauer spectroscopies.

Key words: Nitrogenase – Nitrogen fixation – FeMo enzymes – Oxidation reduction of FeMo cofactor – INDO

1 Introduction

In recent article, Christiansen et al. [1] reported on the changes in the bond distances in the nitrogenase FeMo cofactor (FeMo–co) observed in EXAFS experiments upon partial oxidation and reduction. Interestingly enough, a contraction of the cofactor has been suggested upon reduction as opposed to the generally expected expansion of the system with the addition of electrons. Although small, these changes could be significant for the reactivity of the Mo/Fe/S cluster, limiting the access of the substrate to the active site or making other binding sites available, as discussed widely in the literature [2–4].

Model calculations on the substrate binding to the FeMo–co (Fig. 1) have been done by many groups using various degrees of approximation [5–7]. We have recently examined a theoretical model for the active site of nitrogenase based on the intermediate neglect of differential overlap (INDO) method and reflecting experimental findings for the cofactor from ESR, ENDOR and Mössbauer spectroscopies [8]. We have proposed possible pathways for electron and proton delivery to the cofactor, and initial activation of the N_2 molecule in the interior of the cofactor [8]. This complex is very mobile, and we found the further stages of the N_2 hydrogenation occur outside the FeMo-co, initially on the 4-Fe faces of the cluster [9], in good accord with other theoretical models [5, 6].

A central concern in the reduction of N_2 to ammonia in this process is the order of proton and electron addition to obtain the overall stoichiometry of:

$$N_2 + 8H^+ + 8e^- \rightarrow 2NH_3 + H_2 \quad (1)$$

In this communication, we address the structural changes in the FeMo-co upon reduction as these changes are potentially important for the chemistry involved in the nitrogen fixation. As in our previous work [8], we base our calculations on the INDO Hamiltonian, which has proven useful in a number of recent studies on the structure and spectroscopy of transition-metal systems [10] and iron-sulfur proteins [11]. The model system [8] utilizes the experimental X-ray structure of the cofactor obtained at 2.2 Å resolution [12] and is restricted to the essential atoms in the FeMo-co [8]. The energy of the model cofactor is minimized to the native $S = 3/2$ state of the cofactor using the configuration averaged Hartree-Fock procedure [13] within the restricted open-shell Hartree-Fock(ROHF) approximation, as outlined in detail elsewhere [14]. These calculations start with the given number of electrons, 38 through 43, in the 40 *d*-orbitals of the cluster, using a configuration averaged Hartree-Fock procedure [13] to yield orbitals that are useful in then systematically reducing the system to the lowest energy state. In the "native", 39- electron state, we finally obtain, for example, an ROHF calculated 3 electrons in 3 orbitals quartet state. The stability of this state is further checked with a small Rumer diagram configuration interaction calculation on the ROHF state, and by a projected unrestricted Hartree–Fock (PUHF) [15].

Correspondence to: M.C. Zerner

Table 1. Mulliken charges of the atoms of the FeMo cofactor (FeMo–co) upon oxidation and reduction. Models are designated relative to the native 39-electron state modeled in Ref. [8]; *n* is the number of open-shell electrons in the system. The two different O atoms that ligate to the Mo atom are denoted as CO for the carboxyl, and CC for the non-carboxyl, respectively. The 6-Fe column shows the average charge on the six prismatic, 3-coordinated irons; 9-S* stands for the non-protein, "inorganic" sulfurs

n	Model	O_{CO}	O_{CC}	Mo	N_{His}	Fe_{end}	S_{Cys}	$9 - S^{*}_{av}$	$6 - Fe_{av}$
38	FeMo-le	−0.33	−0.37	1.07	−0.35	1.04	−0.31	−0.70	0.89
39	FeMo-nat	−0.34	−0.41	1.00	−0.34	0.99	−0.48	−0.73	0.86
40	FeMo + 1e	−0.38	−0.39	0.90	−0.33	0.92	−0.55	−0.77	0.82
41	FeMo + 2e	−0.39	−0.42	0.82	−0.32	0.85	−0.68	−0.80	0.78
43	FeMo + 3e	−0.42	−0.44	0.70	−0.29	0.79	−0.71	−0.84	0.74
43	FeMo + 4e	−0.42	−0.49	0.59	−0.27	0.73	−0.73	−0.88	0.69
	Total change	−0.08	−0.08	−0.41	+0.07	−0.26	−0.25	−0.15	−0.17

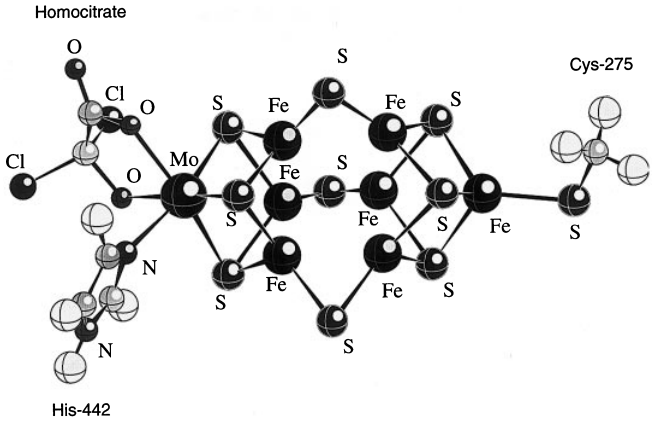

Fig. 1. The structure of the FeMo cofactor found in *Azotobacter vinelandii* and used for these studies. The Cys-275 and His-442 residues are not included in the calculations

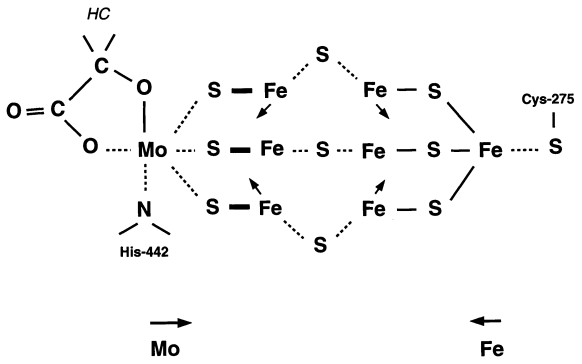

Fig. 2. Illustration of the bond strength changes in the FeMo cofactor upon reduction; numerical data are given in Table 3. *Solid lines* stand for bonds which do not change significantly upon reduction; *broken lines* indicate bond softening with the addition of electrons; bonds in *bold* are those which strengthen in the reduced forms. *Arrows* indicate the directions of movement of the two subsystems upon reduction as obtained from the calculated atomic gradients. These structural changes are more pronounced at the Mo side of the cofactor, the contraction being larger at the two ends of the cluster (see also Table 4)

The one-electron oxidized and reduced species are calculated as triplets, assuming that the more reduced species have gradually descending spin states. We note, however, that the calculated charges and bond indices

Table 2. The multiplicities and relative energies (in eV) compared with those inferred from the experiment (in the brackets) for the FeMo–co

n	Species	Multiplicity	Relative energy
38	FeMo−1e	3 (Integer)[a]	+9.5
39	FeMo−nat	4 (4)[b]	0.0
40	FeMo + 1e	3 (Integer)[a]	−5.2
41	FeMo + 2e	2,4	−7.6, −7.6[c]
42	FeMo + 3e	3	−8.8
43	FeMo + 4e	4	−6.1

[a] Conradson SD, Burgess BK, Holm RH (1988) J Biol Chem 263:13743; for overview, see Burgess BK (1990) Chem Rev 90:1377, pp 1395–1397
[b] Ref. [2]; see also Ref. [8] and references therein
[c] The doublet and quartet are calculated to be nearly degenerate

vary only slightly with the spin state of the model system and the total spin has a marginal effect on the properties under examination in this work.

2 Results and discussion

The results obtained using the ZINDO program [16] are summarized in Tables 1–4 and are illustrated, along with the model structure, in Fig. 2. These calculations are done at fixed geometry. Table 1 provides information on the atomic charges obtained upon electron reduction via Mulliken population analysis [17]. Table 2 shows the multiplicities for which these calculations are reported, and their relative energies. Selected atoms or groups of atoms are given to show the charge distribution in the model cofactor. It is seen from Table 1 that most of the charge, 1.7e out of 4.0e, goes to the sulfur atoms, but a significant amount also populates the metal orbitals – Mo takes 0.4e, the Fe charges decrease by a total of 1.3e, approximately 0.2 electrons/Fe atom. We see from the orbital population analysis that the addition of electrons noticeably affects the metal *d*-orbitals, Mo and Fe, and there is a significant ligand-to-metal back bonding. These changes reflect in the calculated bond indices (see Table 3) and may be important for the substrate reduction and electron/proton affinity of the cluster. We should note that the relative changes in the charge redistribution are more significant for the end atoms of the cofactor, Mo and end- Fe and the S atom which

Table 3. Bond indices between selected groups of atoms in the FeMo–co upon oxidation and reduction. 4Fe—S are the average bond indices between the irons and the sulfurs in the Fe-only subsystem; 3Fe—S are those for the Fe—S bonds in the 3-Fe, Mo cube. S_μ stands for the three S atoms that link the 4-Fe and the 3-Fe, Mo subsystems. Averages of the strengths of the three Mo—S bonds are given in the Mo—S column

Model	Mo—O_{CO}	Mo—O_{CC}	Mo—S	Mo—N_{His}	Fe—S_{Cys}	Fe—S_μ	4Fe—S*	3Fe—S*
FeMo−1e	1.101	1.065	1.067	0.713	1.017	1.148	0.789	0.658
FeMo−nat	1.081	1.003	1.007	0.692	1.019	1.128	0.776	0.661
FeMo + 1e	0.961	1.049	0.991	0.652	1.002	1.103	0.771	0.677
FeMo + 2e	0.937	0.999	0.994	0.631	0.830	1.080	0.766	0.690
FeMo + 3e	0.856	0.981	0.911	0.596	0.790	1.055	0.761	0.702
FeMo + 4e	0.824	0.939	0.758	0.553	0.754	1.034	0.756	0.754

Table 4. Absolute values of atomic gradient changes [Hartree/Å] for the FeMo-co upon 1-electron oxidation and reduction. Models refer to the oxidized, native and reduced system. The two different O atoms that ligate to the Mo atom are denoted CO for the carboxyl, and CC for the non-carboxyl, respectively. The 6-Fe column shows the average gradients of the six prismatic, 3-coordinated irons; 9-S* stands for the non-protein, "inorganic" sulfurs. N_{His} and S_{Cys} refer to the end atoms of the His-442 and Cys-275 residues which approach the cofactor at bonding distances. The gradients for the native state are taken as a reference

Model	O_{CO}	O_{CC}	Mo	N_{His}	Fe_{end}	S_{Cys}	9-S^*_{av}	6-Fe_{av}
FeMo-ox	0.005	0.006	0.022	0.006	0.062	0.032	0.005	0.001
FeMo-nat	0	0	0	0	0	0	0	0
FeMo-red	0.007	0.010	0.041	0.014	0.032	0.003	0.005	0.005

represents the Cys-275 residue (Fig. 2), while the O atoms for the homocitrate (HC) group acquire much fewer of the added electrons upon reduction. It is also notable that the nitrogen belonging to the imidazole (modeling His-442) preserves its negative charge, a change which slightly decreases upon reduction. This has already been observed in the electrostatic potential calculations we reported recently [8], suggesting that this protein link (His-442) might be responsible for the electron delivery to the system. The results given in Table 1 further support this suggestion.

We would also like to point out the greater stability of the reduced states with respect to the semireduced, native state we modeled as containing 39 open-shell electrons [8] (Table 2). The 1e-reduced form has an integer spin, $S = 1$, and is 5.2 eV lower in energy than the reference state. The next 2e-reduced state (which is also consistent with the properties of the native state. [8]; we calculate the $S = 3/2$ and $S = 1/2$ states degenerate, see Table 2) is also of lower energy, followed by the 3e-reduced state which has an integer spin again, $S = 1$, and is again of lowest energy, in line with the expectations from experimental observations [2]. There is presently no evidence on whether these added electrons are immediately utilized in a substrate reduction (N_2 or H^+), or whether they are accumulated in the cofactor prior to the reaction [2]. If the latter is the case, then the reduced species, with their greater stability, might constitute a driving force for the electron transfer to the FeMo-co. It is also possible that the electron transfer could be driven by protonated forms of the cofactor [4b], and this idea will require further attention. Alternatively, if the added electrons are utilized for a substrate reduction, then there has to be a way of "gating" the two competitive reductions in Eq. (1) so as to reach the equilibrium stoichiometry. The ratio between the two reaction products, NH_3 and H_2, is known to vary with the type of bacteria and the metal content of the cofactor [4c].

Non-symmetrical charge distribution within the cofactor is further reflected in the calculated bond indices between the atoms of interest shown in Table 3. The bond index is defined as $B_{AB} = \sum_\mu^A \sum_\nu^B P_{\mu\nu} P_{\nu\mu}$, where P is the first-order density for the symmetrically orthogonalized basis [18], and the sums are restricted to atomic orbitals μ on atom A and ν on atom B. Its value is, for example, three for N_2, two for O_2, etc.

The trends in the bond indices from Table 3 are illustrated in Fig. 2. The first thing to note is the reasonable stability of the structure, even with the addition of 4 electrons. Five of the six bonds that are involved in the co-ordination of the Mo atom weaken noticeably upon reduction the Mo bond with the non-carboxyl O atom of the HC group is only slightly affected. Such a change in the Mo environment may be very important for opening the Mo atom as a possible binding site [2]. especially at the late stages of the nitrogen fixation process [19] when a significant number of electrons have been added to the active site. As the calculated bond indices for the rest of the atoms that surround the cofactor do not change significantly upon reduction, the bond weakening in the ends and in the middle of the cofactor, together with the Fe-S bond strengthening in the 3-Fe, Mo subcube, results in a slight shrinkage of the metal system, as indicated in Fig. 2. The Fe-Fe interactions in the middle of the cofactor are small in magnitude – average indices of 0.2 – and do not change markedly upon oxidation or reduction. These Fe-Fe bonds are expected to make no significant contribution to the small contraction of the metal subsystem upon electron addition. The mode shown in Fig. 2 is accompanied by small rearrangements of the S atoms around the near-threefold axis, which goes from Mo to the end Fe atom of the cofactor. As a result, the molecular volume, calculated using the Van der Waals (VdW) radii of the atoms, decreases upon reduction and increases upon 1-electron oxidation by approximately 1%. Similar changes are also observed for the exposed surface area of the cofactor, calculated from the surfaces of the intersecting VdW spheres. These changes in the geometry of

the cofactor can also be inferred from the calculated differences in the atomic gradients from the reference native state (Table 4). The greater the differences in the atomic gradients, the larger the atom displacements from the reference geometry. Such structural rearrangements can be related to one of the modes suggested by Christiansen et al. [1] (the one in the middle of Fig. 6 of Ref. [1]), and should, according to our calculations, introduce more asymmetry into the system, especially at the Mo side of the cofactor.

The spin densities obtained for the ground states of the 1 electron oxidized, native and reduced forms of FeMo-co have been calculated using the PUHF procedure [15], and are shown in Scheme 1. This approach has proved useful in the description of antiferromagnetically (AF) coupled *d*-electrons in the ground state of model ferredoxins [11]. The spin densities reported in Scheme 1 were obtained from the PUHF Mulliken populations of the α and β orbitals upon projection of the pure spin states from the UHF wavefunction. We note the marked AF spin coupling observed in the cluster, with spins alternating from the histidine to the cysteine end of the structure (the HC group attached to the Mo atom has a very small spin density contribution and is therefore omitted in the scheme) in good agreement with the experimental observations [20]. It is also interesting to note that the total spin density of the central 6-Fe prism is always opposite to that of the end transition metals. The two 3-Fe subsystems have different total spin orientations, again in accord with the experimental studies of the ^{57}Fe hyperfine constants in Mössbauer spectra of FeMo-co showing two different groups of iron atoms in the cofactor with opposite spins [20].

We should mention that the results shown in Scheme 1 reflect the spin densities for a particular spin state ($S = S_z$) obtained after projection from the UHF wavefunction. Other spin states, however, could possibly be involved – such as $S = 1/2$ for the native state [2, 3] – and may contribute to the total spin distribution in the cofactor. No trapped valencies were observed for the iron atoms in the present calculations as also concluded from the experimental work of others [20]; some of the Fe atoms are seen intermediate between Fe(II) and Fe(III), while others are closer to Fe(III) which seems to be the dominant oxidation state for the central 6-Fe prism. The end-Fe atom is closer to Fe(II) and is markedly affected by the 1-electron oxidation or reduction (see Scheme 1). The UHF calculations show two distinct spin orientations for Fe atoms located in both subcubes, with Fe atoms apparently AF coupled through the intracube sulfurs and the three μ-S atoms that link the two cubes. Changes in the oxidation state are, however, more pronounced for the Mo-cube than that which is Fe-only. This is in line with the previous observations on the atomic charges and bond indices given above. The calculated spin density on the Mo atom is close to 2, in agreement with the assumption that Mo is in formal oxidation state +4 [2, 21].

Scheme 1. Calculated atomic spin densities

$$1e^{-}OX\ (S=1)\quad His-N^{\downarrow}_{-0.1}-Mo^{\uparrow}_{+1.9}-3S^{\downarrow}_{-0.2}-3Fe^{\downarrow}_{-0.9}-3S^{\downarrow}_{-0.7}-3Fe^{\uparrow}_{+0.4}-3S^{\uparrow}_{0.04}-Fe^{\uparrow}_{+2.2}-S^{\downarrow}_{-0.5}-Cys$$

$$NATIVE\ (S=3/2)\quad His-N^{\downarrow}_{-0.1}-Mo^{\uparrow}_{+1.8}-3S^{\downarrow}_{-0.2}-3Fe^{\downarrow}_{-1.2}-3S^{\downarrow}_{-0.1}-3Fe^{\uparrow}_{+0.5}-3S^{\uparrow}_{+0.1}-Fe^{\uparrow}_{+2.7}-S^{\downarrow}_{-0.6}-Cys$$

$$1e^{-}RED\ (S=1)\quad His-N^{\downarrow}_{-0.1}-Mo^{\uparrow}_{+1.9}-3S^{\downarrow}_{-0.2}-3Fe^{\downarrow}_{-1.9}-3S^{\downarrow}_{-0.2}-3Fe^{\uparrow}_{+0.4}-3S^{\uparrow}_{0.01}-Fe^{\uparrow}_{+2.2}-S^{\downarrow}_{-0.5}-Cys$$

The AF exchange is known to be structure dependent and the observed spin conjugation may vary upon conformational changes. Small structural changes, as those observed experimentally and examined theoretically here, do not affect measurably the AF coupling and the trends in the spin densities upon 1-electron oxidation and reduction. However, spin distributions upon major conformational changes, if any, should be treated with caution and need to be examined separately.

It is interesting to note before concluding that the 41-electron (in 40 *d*-orbitals) species designated as FeMo + 2e has lower absolute energy than that which we have called "native". This species has a low energy quartet, and is also a candidate for the "native" form. It has similar magnetic, Mössbauer and structural properties to the 39-electron complex, as discussed in some detail in Ref. [8]. One might predict, however, that if this species were the "native" one, the addition of N_2, or even the addition of N_2 and one or more protons, might be required before the addition of electrons. The reason for this is apparent from Table 2. There is a great energy advantage for the 39-electron complex to add an electron, −5.2 eV, while the stabilization achieved in going from the 41-electron to the 42-electron species is smaller, although still negative at 1.2 eV.

Acknowledgements. We are very grateful to Dr. Marshall Cory (UF) for his continuing support of this project through the many valuable discussions we had on model ferredoxins and nitrogenase clusters. This work was supported in part through a grant from the Office of Naval Research and through a grant from the National Science Foundation, CHE-9312651. We acknowledge also a SUR 1996 grant from IBM.

References

1. Christiansen J, Tittsworth RC, Hales BJ, Cramer SP (1995) J Am Chem Soc 117:10017
2. Burgess BK, Lowe JL (1996) Chem Rev 96:2983; Burgess BK (1990) Chem Rev 90:1377
3. Howard JB, Rees DC (1996) Chem Rev 96:2965
4. (a) Sellmann D (1993) Angew Chem Int Ed Engl 32:64; (b) Sellmann D, Becker T, Knoch F (1996) Chem Eur J 2:1092; (c) Eady RR (1996) Chem Rev 96:3013; for overview on metals in biology, also Holm RH, Kennepohl P, Solomon EI (1996) Chem Rev 96:2239
5. Deng H, Hoffmann R (1993) Angew Chem Int Ed Engl 32:1062
6. Dance IG (1994) Aust J Chem 47:979
7. Machado FBC, Davidson ER (1995) Theor Chim Acta 92:315
8. Stavrev KK, Zerner MC (1996) Chem Eur J 2:83
9. Stavrev KK, Zerner MC (1996) 212th Natl ACS Meeting, Orlando, Florida; Detailed work on this subject which includes INDO and density functional theory calculations is in preparation
10. Stavrev KK, Zerner MC (1995) Chem Phys Lett 233:179; Stavrev KK, Zerner MC (1995) J Chem Phys 102:34; Stavrev KK, Zerner MC, Meyer TJ (1995) J Am Chem Soc 117:8684
11. Stavrev KK, Zerner MC (1995) Int J Quantum Chem: Quantum Biol Symp 22:155; Cory MG, Stavrev KK, Zerner MC (1997) Int J Quantum Chem 63:781
12. Chan MK, Kim J, Rees DC (1993) Science 260:792
13. Zerner MC (1989) Int J Quantum Chem 35:567; see also, McWeeny R (1989) Methods of molecular quantum mechanics, 2nd edn. Academic Press, London
14. Estiu G, Zerner MC (1994) J Phys Chem 98:4793; (1994) J Phys Chem 98:9972
15. For PUHF methodology, see Harriman JE (1964) J Chem Phys 40:2827; Phillips DH, Schug JC (1974) J Chem Phys 61:1031, and references therein; Zerner MC, Cory MG (in preparation)
16. Zerner M, ZINDO program package, Quantum Theory Project, University of Florida, Gainesville, Florida; see also, Zerner MC, Loew GH, Kirchner R, Müller- Westerhoff U (1980) J Am Chem Soc 102:589; Ridley JE; Zerner MC (1973) Theor Chim Acta 32:118; Bacon AD, Zerner MC (1979) Theor Chim Acta 53:21
17. For Mulliken population analysis we assume that the basis employed for the calculations is related to Slater-type orbitals through symmetric orthogonalization
18. For a review on bond index analysis, see Sannigrahi AB (1992) Adv Quantum Chem 23:302
19. Demadis KD, Malinak SM, Coucouvanis D (1996) Inorg Chem 35:4038; Malinak SM, Simeonov AM, Mosier PE, McKenna CE, Coucouvanis D (1997) J Am Chem soc 119:1662
20. True AE, Nelson MJ, Venters RA, Orme-Johnson WH, Hoffmann BM (1988) J Am Chem Soc 110:1935; Rawlings J, Shan VK, Chinsell JR, Brill WJ, Zimmermann R, Münck E, Orme-Johnson WH (1978) J Biol Chem 253:1001; for overview, see Stiefel EI, George GN (1994) In: Bertini I, Gray HB, Lippard SJ, Valentine JS (eds) Bioinorganic chemistry. University Science, Mill Valley, California, p 365
21. Coucouvanis D (1993) In: Stiefel EI, Coucouvanis D, Newton WE (eds) Molybdenum enzymes, cofactors, and model systems. American Chemical Society, Washington, DC, p 304 and references therein